Istituto Nazionale di Ricerca Metrologica - INRiM

E. Biolcati, A. Germak, F. Mazzoleni, C. Origlia, S. Palumbo, F. Vitiello

Absolute measurements of the free-fall acceleration in Esch-sur-Alzette, Belval, Luxembourg EURAMET.M.G-K2 2015

Technical Report RT-10/2016 (March)

Abstract

The described work was carried out on November 2015 by the Istituto Nazionale di Ricerca Metrologica (INRiM) of Turin (Italy), for the participation of the IX Regional Comparison of Absolute Gravimeters EURAMET.M.G-K2 (former ECAG2015) in the dedicated laboratory of Belval centre, in Esch-sur-Alzette, Luxembourg, organized by the University of Luxembourg.

The experimental results of the absolute measurement of the free-fall acceleration g in the three sites dedicated to the comparison are reported. The measurements were performed with the transportable absolute gravimeter IMGC-02 of the INRiM. At the same time, 20 other absolute gravimeters coming for different parts of the Europe and United States were used for the comparison. In the proximity of the measurement sites, a relative gravimeter and an absolute one were enabled to monitor the variation of the gravitation field along the days.

With the IMGC-02 instrument a relative accuracy of few parts in 10^9 is reachable, i.e. measurement of g with uncertainty of tens microgals ($1\ \mu\text{Gal} = 1 \times 10^{-8}\ \text{m s}^{-2}$).

$\sim \cdot \sim$

Il lavoro qui descritto è stato svolto nel mese di novembre del 2015 dall'Istituto Nazionale di Ricerca Metrologica (INRiM), per partecipare al IX Confronto Internazionale dei Gravimetri Assoluti EURAMET.M.G-K2 (ex ECAG2015). Esso ha avuto luogo nel centro polifunzionale di Belval, presso Esch-sur-Alzette, Lussemburgo ed è stato organizzato dall'Università del paese ospitante.

Si riportano i risultati sperimentali della misura assoluta dell'accelerazione locale di gravità g nei tre siti dedicati per il confronto. Le misure sono state realizzate con il gravimetro assoluto trasportabile IMGC-02 dell'INRiM. Contemporaneamente, altri 20 gravimetri provenienti da diverse parti d'Europa e dagli Stati Uniti sono stati utilizzati per il confronto. In prossimità dei siti di misura, era attivo un gravimetro relativo e uno assoluto per controllare le variazioni del campo gravitazionale giorno per giorno.

Con l'IMGC-02 si raggiunge un'accuratezza relativa di qualche parte in 10^9, ovvero misure di g con incertezza di decine di microgal ($1\ \mu Gal = 1 \times 10^{-8}\ m\ s^{-2}$).

Contents

List of Tables

List of Figures

1 IMGC-02 absolute gravimeter

1.1 Operating principle

The absolute measurement of the free-fall acceleration, g, was performed with the prototype apparatus developed by INRiM [1, 2]. It is shown in figure 1. The g value is measured by tracking the vertical trajectory of a test-body subjected to the gravitational acceleration. The IMGC-02 adopts the symmetric rise and falling method, where both the rising and falling trajectories of the test-body are recorded. The raw datum consists in an array where each element represents the time correspondent to the passage of the test-body through equally spaced levels (or stations). A linear model function is fitted to the raw data in a least-squares adjustment. One of the parameters of the model is the acceleration experienced by the test-body during its flight. A measurement session consists of about 1000 launches taking during about 10 hours, in order to be able to reduce the effect of the very low frequency Earth oscillations. The measurement session is carried out during the night to have the minimum human noise effect.

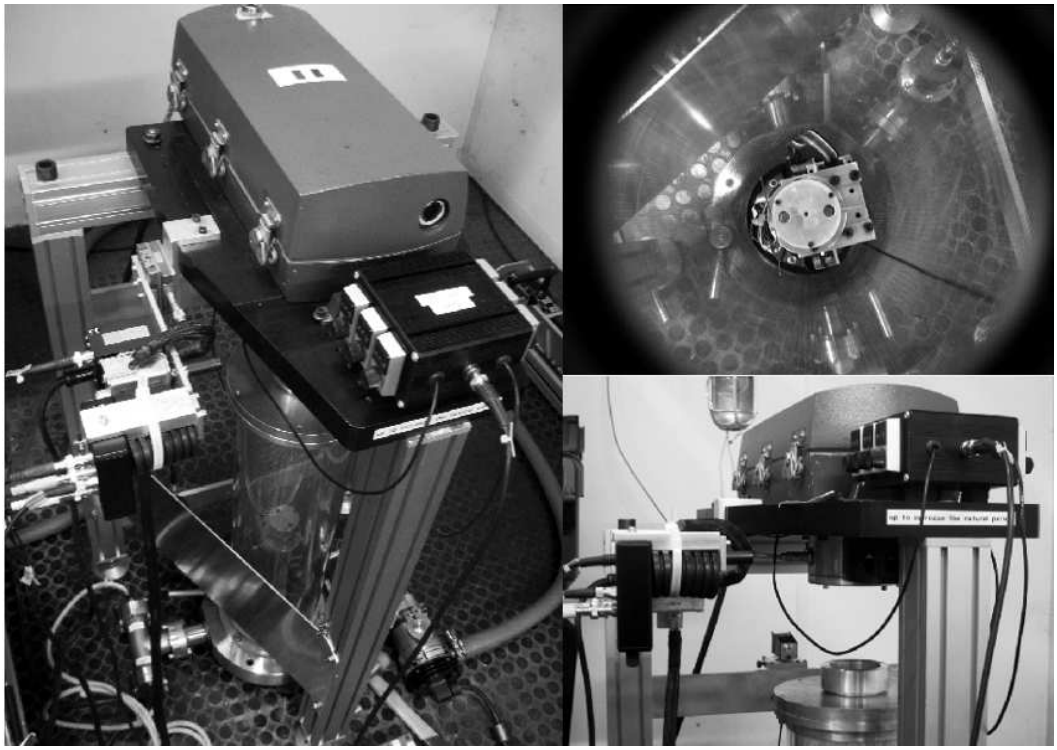

Figure 1: Pictures of the IMGC-02 absolute gravimeter. Left panel: the whole apparatus made of vacuum chamber and measurement system. Right panel, up: inside part of the vacuum chamber with test object. Right panel, down: detail showing quad-cell and photomultiplier detector, interferometer box, seismometer, piezo-electric control, laser fiber support.

A schematic layout of the apparatus is shown in figure 2. The main parts of the instrument are a Mach-Zehnder interferometer [3] and a long-period (about 20 s) seismometer. The wavelength of a iodine stabilised He-Ne laser (Winters Electo-Optics, model E100 137. Last calibration: INRiM, 2005) is used as the standard length. The inertial mass of a seis-

mometer supports a corner-cube reflector, which is the reference mirror of the interferometer. The moving mirror of the interferometer is a corner-cube retro-reflector too and is directly subjected to the free falling motion. It is thrown vertically upwards by means of a mechanical launch pad in a vacuum chamber. Interference fringes emerging from the interferometer are detected by a photo-multiplier. The output signal is sampled by a high-speed waveform digitizer synchronized to a Rubidium oscillator (Symmetricon 5178. Last calibration: INRiM, 2012). It is used as the time standard. Equally spaced stations are selected by counting a constant integer number of interference fringes N_f that is usually 1024. Thus consecutive stations are separated by a distance $d = N_f\lambda/2$, being λ the wavelength of the laser radiation.

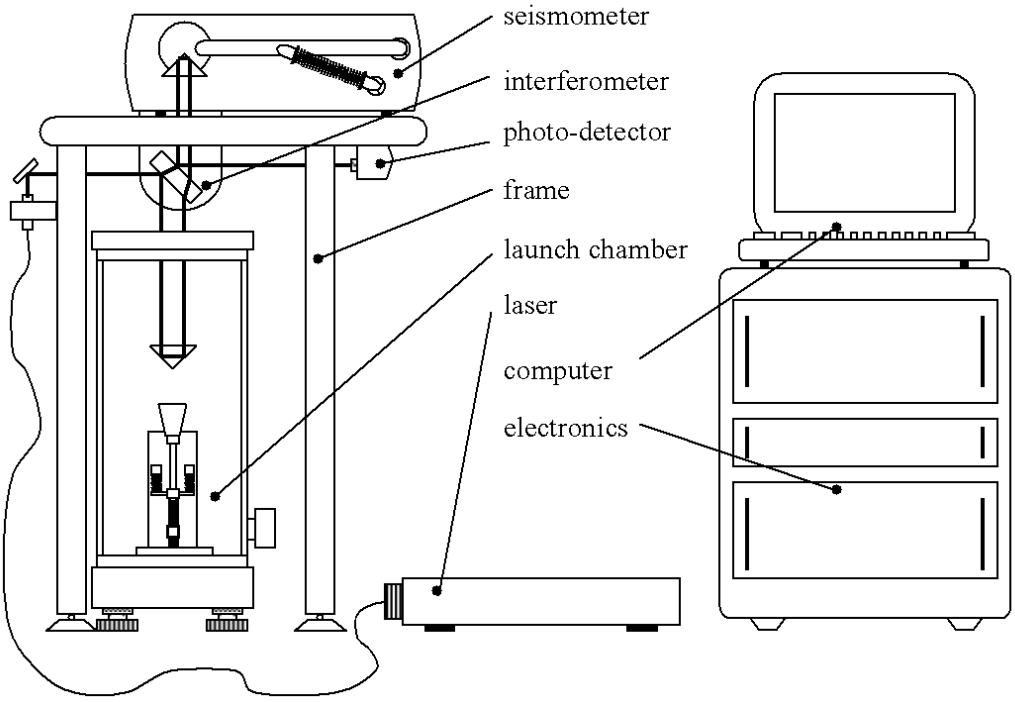

Figure 2: Layout of the IMGC-02 absolute gravimeter.

The so called *local fit method* is used to time the interference signal [4]. The time is computed by fitting the equation model of the interference of monochromatic waves to the interference fringe correspondent to the selected station. The space-time coordinates are processed in a least-squares algorithm, where a linear model function is fitted to the trajectory [5]. Each drop gives an estimate of the g value.

A dedicated computer manages the instrument. The pad launch is triggered when the system is found to be ready. The software checks the pad launch state (loaded or unloaded) and the laser state (locked or unlocked). Environmental parameters such as the local barometric pressure and the temperature are acquired and stored for each throw.

The software `GravisoftM` drives the instrument and stores the measurement data. It was developed on the LabVIEW® platform. Data are then post-processed by using `absinthDataProcess.C` and `absinthFinalDraw.C` macros to apply all the corrections and compute the value of g. Such programs are written in C++ language and exploit CERN-

ROOT libraries [6].

The following geophysical corrections are applied: (i) the Earth tides and ocean loading are computed with the ETGTAB® (version 3.10 19950123 Fortran 77); (ii) the polar motion correction is computed starting from the daily pole coordinates x and y obtained from the International Earth Rotation Service (IERS) [7]. The gravitational acceleration is normalized to a nominal pressure. Instrumental corrections are also applied to take into account for parasitic effects as the laser beam verticality and divergence.

The g value associated to every measurement session is calculated as the arithmetic mean of N measurements and it is referred to a specific height from the floor h_{ref}. The expanded uncertainty is evaluated according to the ISO GUM guide [8] and the method is described in the next section.

1.2 Uncertainty

The uncertainty associated to the g measurement is evaluated by combining the contributions of uncertainty of the IMGC-02 absolute gravimeter, called *instrumental uncertainty*, to the contribution of uncertainty depending on the observation site [1].

1.2.1 Instrumental uncertainty

Influence factors which are characteristic of the instrument and are not negligible with the actual performances are listed in the following.

- *Temperature gradient.* A temperature gradient ΔT of the residual air generates a pressure gradient on the test body. The consequent acceleration coming by the ideal gas law is $a_{\mathrm{temp}} = \Delta T\, P\, A/(T\, m)$ where A is the section of the test body.

- *Self attraction.* The mass of the parts constituting the apparatus (such as seismometer, structure, vacuum chamber, etc.) are sources of a gravitational field, which can systematically perturb the motion of the flying object. The acceleration generated by each part of the instrument is given by $a_{\mathrm{mass,i}} = G\, M_i/z_i^2$ with G the universal gravity constant, M_i the mass of the part i, z_i the distance between the centre-of-mass of the part i and the test object at its measurement height [9].

- *Laser beam verticality.* A residual angle ϑ between the laser beam and the vertical direction modifies the value of g as follows (approximation for small angles is used): $\Delta g/g \simeq \vartheta^2/2$. The bias is then systematically negative and proportional to the square of the misalignment angle value. The probability distribution function (PDF) of such error is not centred at zero, due to the complexity of the system. For this reason, a correction for this error should be taken into account in the calculation of the final value.

- *Laser accuracy.* Each laser has a proper uncertainty associated to the accuracy of the frequency. On the other hand, the time stability of this accuracy has to be analyse too in order to check for any possible drift effect.

- *Laser beam divergence.* A Gaussian laser beam has a non-zero curvature of wave fronts. It leads to systematic biases similar to those arising from the non-verticality. When

the wave fronts is curved, only the axis of the beam can be aligned on a interferometer. The remaining parts of the beam are inherently misaligned, changing the effective wavelength λ value which could require a dedicated correction as: $\Delta g/g = \Delta\lambda/\lambda \simeq \lambda^2/(4\pi^2\omega_0^2)$ where ω_0 is the waist.

- *Clock delay.* The Rb oscillator was calibrated using the Cs oscillator of the INRiM. However, the associated uncertainty and the time drift effect must be considered.

- *Retro-reflector balancing.* The dynamic equations of the test body are referred to its centre-of-mass, while the experimental trajectory is tracked relates to the optical centre of the corner-cube prism. If rotations occur during the flight, the trajectory accuracy is affected by a systematic bias related to the distance d between the two centres. The parasitic acceleration is given by: $a_{\text{cen}} = \omega^2\, d$ where ω is the angular velocity of the object.

- *Reference height.* Each launch statistically reaches a different maximum height. As a consequence, the height whose the g value is referred changes time by time. An averaged value is given as reference height and the uncertainty associated on g is calculated.

Other factors as vacuum level, non-uniform magnetic field, electrostatic attraction, overall drift, air gap modulation, length and time standards and radiation pressure have been studied in details and they are found to be negligible with a respect to the expected uncertainty.

Table 1 reports the quantitative assessment of effects and corrections described above. The expanded uncertainty at the 95% confidence level (coverage factor k = 2.1 and 17 degrees of freedom) is estimated to be $U = 7.9$ μGal.

Instrumental uncertainty

x_i	type	corr.	a_i or s_i	$\partial y/\partial x_i$	dof	u_i / μGal
temperature	B - U	0	0.15 μGal	1	10	0.11
laser verticality	B - rect.	0.66 μGal	0.21 μGal	1	15	0.12
laser accuracy	A	0	0.1 μGal	1	30	0.1
beam divergence	A	5.2 μGal	0.52 μGal	1	10	0.52
clock delay	A	0	0.6 μGal	1	30	0.6
reflector balancing	B - rect.	0	0.0001 m	6.3×10^{-4}	15	3.6
reference height	B - rect.	0	0.0005 m	3.0×10^{-6}	30	0.09
self-attraction	A	0.7	0.1 μGal	1	30	0.1
total correction		6.6 μGal				
combined uncert.						3.7 μGal
	degrees of freedom		17			
	confidence level		95%			
	coverage factor		2.1			
	expanded uncertainty		7.9 μGal			

Table 1: Instrumental uncertainty of the IMGC-02. Drag, out gassing, magnetic and electrostatic field, air gap modulation, refraction index, fringe timing and radiation pressure are negligible for the budget uncertainty (1 μGal = 1×10^{-8} m s^{-2}).

Only the non-negligible contributions are reported. In the second column, the type of the error is indicated together with its probability distribution: U stays for U shape, *rect* for rectangular one. The degrees of freedom are calculated using the Welch-Satterthwaite formula, whilst the coverage factor comes from the t-Student distribution.

1.2.2 Site-dependent uncertainty

The main factors depending from the observation site are the following ones.

- *Coriolis force.* Each object moving relative to the Earth is subjected to the Coriolis acceleration, described as: $a_{\mathrm{Cor}} = 2\,\omega_E\,v_{EW}\,\sin(\pi/2 - \varphi)$, where ω_E is the Earth angular velocity, v_{EW} the velocity induced by the Coriolis effect, φ the latitude of the measurement site.

- *Barometric pressure.* Each g value is normalized to a nominal pressure: $\Delta g = f_B(P_{\mathrm{obs}} - P_{\mathrm{nom}})$ with $P_{\mathrm{nom}} = 1013.25(1 - h_m/44330.77)^{5.2559}$. P_{obs} is the pressure value measured during the measurement session, $f_B = 0.30$ μGal$\cdot$ mbar is a barometric factor recommended by IAG 1983 and h_m the topographic elevation of the site.

- *Tide and ocean loading.* The gravity tide effect and the consequent ocean loading give the highest correction to each g value. However, the ETGTAB software allows a very detailed description of such effect with well known uncertainty contribution.

- *Standard deviation of the mean.* The standard deviation takes into account all the statistic contributions. In particular the low frequency oscillation effect which are not filtered by the seismometer is significantly reduced.

Floor recoil effect and the polar motion correction give an uncertainty contribution which results to be negligible for our purposes. In table 3 all the contributions are summarized for the observation sites of this technical report. Usually, for sites as dedicated laboratories with very stable floor, the final expanded uncertainty combined with the instrumental one is less than 9 μGal.

2 Experimental results

In the following the measurement site will be briefly described. The data taking operation performed in Luxembourg will be explained in the next section. After that, three separately sections will be dedicated to the analysis of data taken in the three measurement sites of the comparison. In those parts values, corrections and uncertainty calculations will be reported. Lastly general considerations about the IMGC-02 performance will be discussed in relation to the measurements done in the INRiM gravity laboratory before and after the comparison.

2.1 Measurement site

The usual site used in the past for Regional and International Comparison of Absolute Gravimeters was not available for logistic problems. The organizers found a reasonable alternative: the recent building constructed in Belval, Esch-sur-Alzette, of the University of Luxembourg. The geographical position of the laboratory is shown in figure 3.

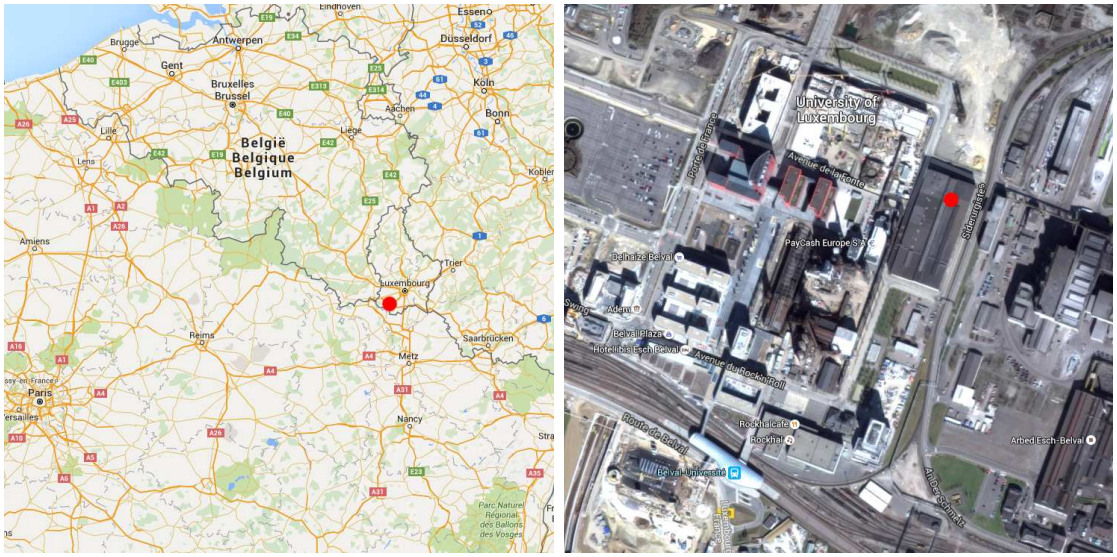

Figure 3: EURAMET.M.G-K2 2015 measurement site location obtained using Google Maps.

It consists in a large area dedicated to measurements of the stability of big machineries. It is not isolated, but very close to mall, shops, offices and university rooms. Men at works were also present in close construction sites. The human noise is then reduced during the night only.

The floor is optimized for different purposes and it is not appropriate for alignment operations of the gravimeters. For this reason and for the non negligible human noise such operations were very hard. The rise and fall absolute gravimeters are more sensitive to this kind of problems than the free fall instruments. Hence, the scatter of the IMGC-02 is worst with a respect to usual measurement sites.

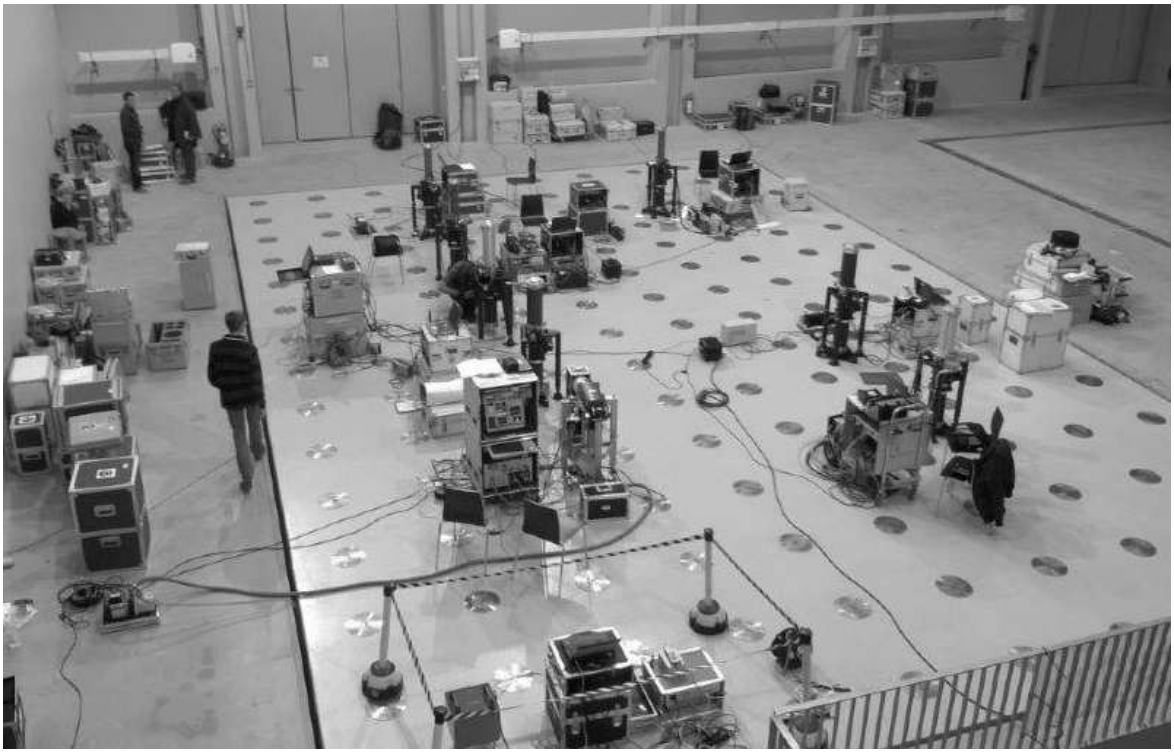

Figure 4: EURAMET.M.G-K2 2015 measurement site. The orientation of the IMGC-02 absolute gravimeter is observable.

2.2 Data taking

The measurements were taken on the nights and days between the 12^{th} and the 15^{th} of November 2015. People from INRiM involved in the data taking procedure were Emanuele Biolcati, Alessandro Germak and Claudio Origlia.

In figures 4, the position and the orientation of the IMGC-02 is shown for a measurement site. The arm of the seismometer was oriented in the North-South direction. We performed three data sessions of measurements in three different points. Results will then used for the comparison as done in previous comparison. An example of the usual data processing is present in [10, 11].

In all the data sessions, the instrument processed and stored more than 1000 trajectories. Outliers are found by applying the so called 3-sigma criterion to the g values. The final value was extracted from the mean of the acceleration values coming from each drop.

We arrived on the 9^{th} of November at 5 p.m., we mounted the whole apparatus and we switched on the vacuum pump system. The first night was dedicated to the warm-up phase of the instrument.

Every component of the IMGC-02 was found in the nominal status. The He-Ne laser reaches the nominal equivalent power of 4.1 V. The seismometer period resulted to be of 18.2 s. The pillar to floor height was 73.3 mm. The pressure in the vacuum chamber reached nominal level during the night: $p = 2.5 \times 10^{-5}$ mbar. Temperature oscillations of about one degree were recorded, due to the opening of the door of the building.

During the three nights, the apparatus experienced a scatter of the values of about 30÷35 μGal. The averaged trajectory residuals after the measurement sessions are within 5 nm. The fraction of accepted drops (i.e. no problem in the local fit method) equals 90÷92 %. During the day, we operated in the moving of the instrument between measurement sites and we fine tuned the working parameters of the IMGC-02.

Measurements were performed in three different sites and for each of them we have several dataset. In table 2 the characteristics of the recorded datasets are listed.

site	date	time	drops	dataset	notes
s10	10.11	morning	259	20151301	warm-up effect
s10	10.11	afternoon	622	20151302	used
s10	10.11	night	1601	20151303	misalignment
s4	11.11	afternoon	891	20151304	not stable
s4	11.11	night	1656	20151305	used
s7	12.11	morning	354	20151306	alignment test
s7	12.11	afternoon	372	20151307	not stable
s7	12.11	night	1385	20151308	used

Table 2: Datasets taken in the three different sites at Belval.

Data were stored in a portable hard disk and roughly processed with a dedicated laptop to check for the goodness of the results in term of instrument stability, tide corrections and parasitic effects. Data are then processed again in Turin applying all the corrections and statistical criteria to reject outliers.

2.3 Data analysis

For each drop, the trajectory is reconstructed starting from the N time values T_i recorded by the instrument. The relative space coordinate is obtained as $S_i = iN_f\lambda/2$, where λ is the wavelength of the He-Ne laser and $N_f = 1024$ is the sampling factor. The linear least square algorithm allow us to compute the fit function defined as:

$$z(t) = S_0 + V_0 t - \frac{1}{2} g t^2, \tag{1}$$

using z_0, v_0, g_0 as free parameters. This is a simplification of the problem, because a step d is also present between the two branches and the time values must be referred to the apex coordinate t_a. More details are present in [5]. It is possible to calculate the trajectory residuals as $r_i = S_i - z(T_i)$ for the N couples of coordinates.

The behaviour and the distribution of such residuals is strictly correlated to the goodness of the drop in term of verticality of the launch, noise due to external source and unknown parasitic effects too. For this reason, as a quantitative probe of this goodness the standard deviation s_r of the residual distribution is stored for each drop.

In order to monitor the operating of the IMGC-02 during the measurement data session, several quantities are checked as a function of the time and the drop number. The main ones are also shown in such report: (i) initial velocity V_0; (ii) $h_{\text{eff}}/z_{\text{apex}}$ ratio; (iii) uncertainty due to the remaining step between branches u_{step}; (iv) velocity-proportional component a_{vel}.

The V_0 is directly extracted from the linear least square algorithm as one of the free parameters of equation 1. Its behaviour reflects the warm-up status of the launch system springs, hypothetically strong dependences on temperature gradient and unexpected fit failures.

The effective height is calculated as

$$h_{\text{eff}} = \frac{H}{3T^2} G(T_i, T_i^4) \tag{2}$$

where H is the total analyzed height, T the total analyzed time, $G(X, Y)$ is the least square operator using the notation suggested in [5]. In this case it is used with variable T_i and T_i^4 to calculate a particular weighted function. The vertical coordinate of the apex is geometrically calculated using the parabola curve. The ratio between such quantities give an accurate determination of the factor to use to estimate the reference height as $h_{\text{ref}} = h_{\text{apex}} - h_{\text{eff}}$. The value should be close to the one calculated for an infinite number of equally spaced levels that is 1/6.

In the linear model algorithm, a reiterative method is dedicated to reduce the intrinsic spatial step between the two branches of the trajectory. The uncertainty due to the remaining step is calculated as

$$u_{\text{step}} = d \cdot G(T_i, S_i^{01}) \tag{3}$$

where d is the spatial step and $G(T_i, S_i^{01})$ is here used to calculate the first derivative of the weighted function at the apex, as described in [5]. Usually it is less than 0.25 μGal and it is a probe of the working of the step reduction algorithm.

The rise-and-fall gravimeter allows us to calculate the component of the acceleration that is dependent on the velocity. Such component includes the contribution due to the residual gas in the vacuum chamber, the one coming from the effects of finite speed of light, other

minor influences as electrical and magnetic fields. The component is so obtained from the difference between the values of g calculated during the rise and fall separately. It is obtained as:

$$a_{\text{vel}} = \frac{7\,T}{192\,H}\,(g\uparrow - g\downarrow)\,G(T_i, T_i^3) \tag{4}$$

where $G(T_i, T_i^3)$ is the central moment of the weighted function [5]. The value is several orders of magnitude less than the g value. It is a probe of the pressure level in the vacuum chamber and of unknown parasitic effects.

2.3.1 Site 10

The first dataset 20151301 was not used to calculate the g value because still affected by the warm-up phase. The one taken during the night, dataset 20151302, presents no problem and enough number of drops. It was used to calculate g. The dataset 20151303 was affected by strong misalignment during the night, so data are not taken into account for the analysis.

In figure 5 (right) the values of g coming from the first measurement site s10 are shown as a function of the time (i.e. the drop number). A quite stable behaviour is visible and no systematic accumulation is present. In the left panel the distribution of the values is shown together with a superimposed Gaussian fit function.

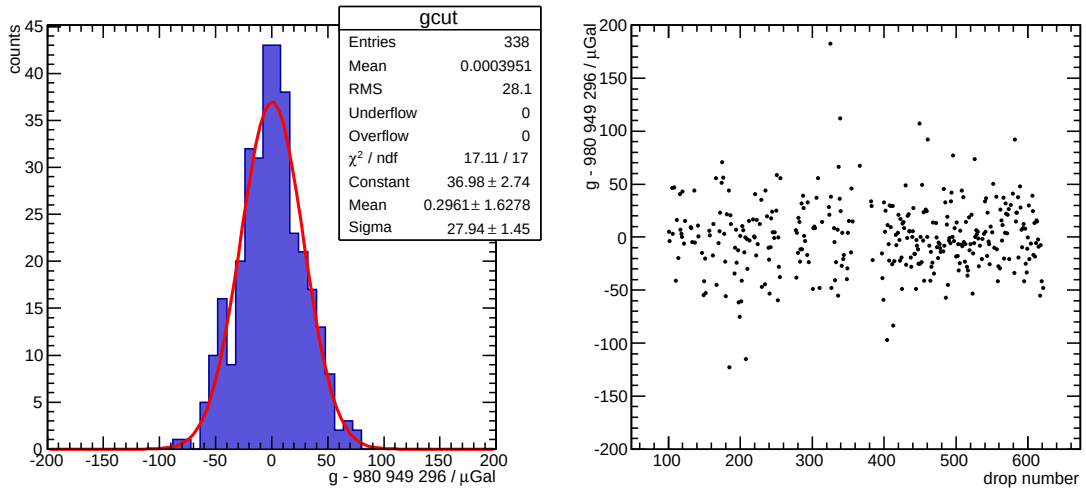

Figure 5: Experimental results for the site 10, folder 20161302. Values of g (subtracted to a nominal value for visibility) versus launch number (right). Distribution of the those values with Gaussian fit superimposed (left).

In figure 6 (left) the values of g versus the standard deviation of the residual distributions are shown. Because no correlation is evident, a cut on the s_r does not bias the mean value of g. In the right panel, the distribution of the s_r is shown. A tail for values higher than 6 is observable. For this reason we rejected all drops with s_r higher than 6 because they were not taken in the optimal instrumental and geophysical conditions. Applying such cut the distribution follows a more Gaussian behaviour.

In figure 7 it is possible to see the behaviour of four quantities used to monitor the operating of the IMGC-02 during the whole dataset a function of the drop number. The velocity is constant in time, without unexpected effects. The $h_{\text{eff}}/z_{\text{apex}}$ ratio is uniformly distributed around the nominal value of 1/6 used to calculate the reference height. The uncertainty due to the remaining step between rise and fall branches of the trajectory is centered at zero and is lower than ± 0.03 μGal, so as to be negligible with a respect to the final uncertainty on g. In the same way, the contribution due to terms that are proportional to the velocity are few order of magnitude less to the value of gravity acceleration.

In figure 8 the environment parameters and tide effect are shown as a function of the time. The conditions were quite stable during the whole data session.

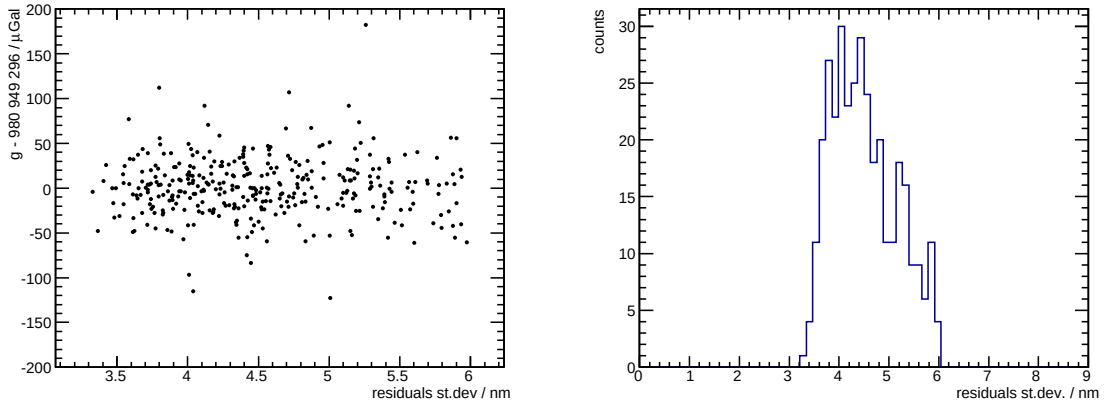

Figure 6: Experimental results for the site 10, folder 20161302. Values of g (subtracted to a nominal value for visibility) versus s_r of the residual distributions (left). Distribution of the s_r values (right).

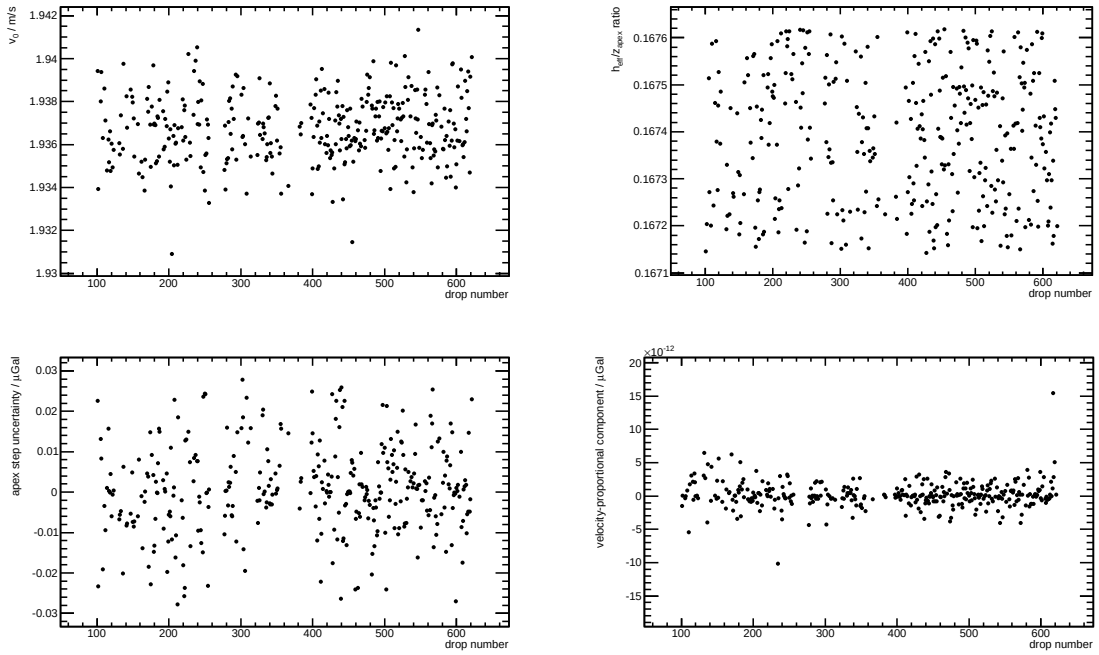

Figure 7: Measurement monitoring quantities coming from linear model algorithm for the site 4: initial velocity (up, left); ratio between the effective height and the apex vertical coordinate (up, right); uncertainty due to the remaining step between the two trajectory branches (down, left); contribution due to the component proportional to the velocity (down, right).

The measurement uncertainty for the site 10 is summarized in table 3. It includes the instrumental uncertainty reported in table 1.

Only the non-negligible contributions are reported. In the second column, the type of the error is indicated together with its probability distribution: *U* stays for *U* shape, *rect*

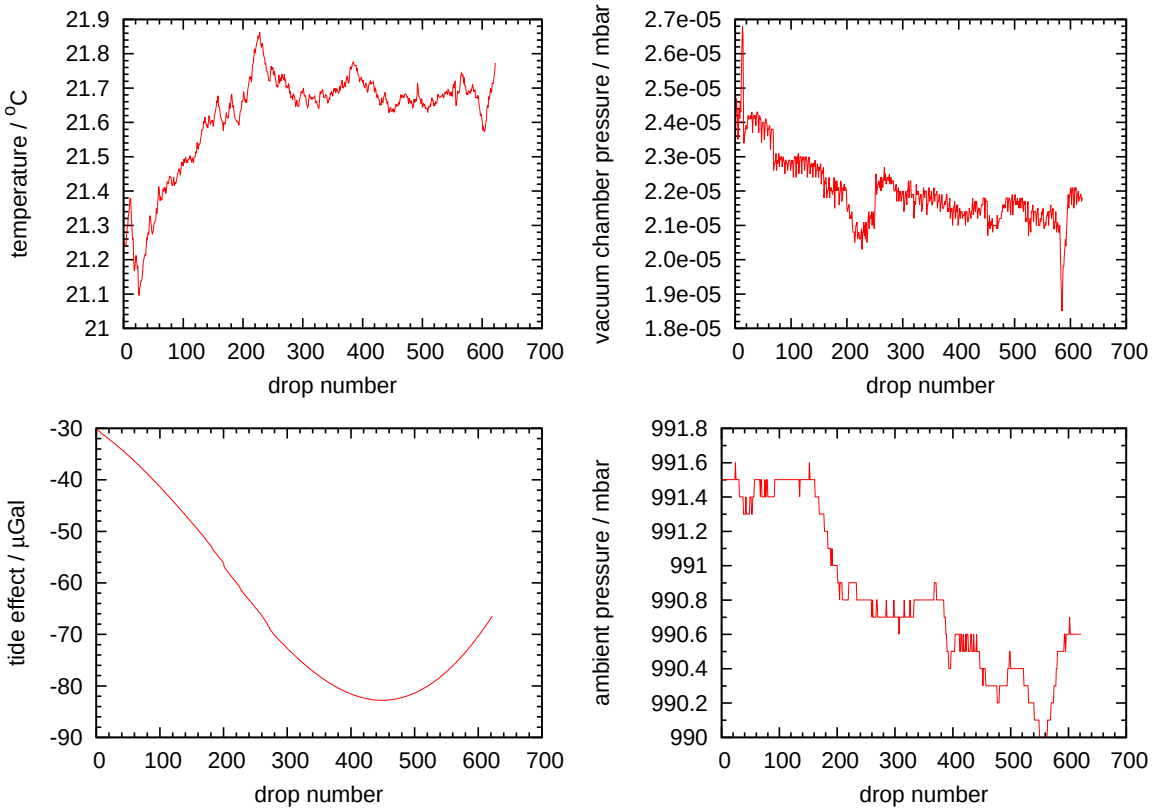

Figure 8: Experimental parameters recorded at the site 10 during the measurement session. Ambient temperature, barometric pressure and tide effect versus the drop number.

for rectangular one. The degrees of freedom are calculated using the Welch-Satterthwaite formula, whilst the coverage factor comes from the t-Student distribution.

In table 4 the most important results and parameters are listed for the first measurement site s10. The vertical gravity gradient calculated by the EURAMET organizers is also reported, but it was not used in the analysis of IMGC-02 data.

Measurement uncertainty for the site 10

x_i	type	corr.	a_i or s_i	$\partial y/\partial x_i$	dof	u_i / μGal
instrumental	A	0	3.7 μGal	1.0	17	3.7
Coriolis force	B - rect.	0	2.8 μGal	1.0	10	1.4
barometric pressure	B - rect.	4.6 μGal	1.0 μGal	1.0	15	0.58
tide	A	-52.2 μGal	0.3 μGal	1.0	15	0.3
ocean loading	A	0	0.2 μGal	1.0	15	0.2
standard dev. mean	A	0	1.5 μGal	1.0	337	1.5
total correction		-48.4 μGal				
combined uncert.						4.3 μGal
		degrees of freedom	30			
		confidence level	95%			
		coverage factor	2.1			
		expanded uncertainty	8.8 μGal			

Table 3: Final uncertainty for the absolute measurement at s10 in Belval. Floor recoil effect and polar motion correction (0.6 μGal) are negligible for the budget uncertainty.

Summary for the site 10

Data taking start (UTC)	10-11-2015 17:15
Data taking stop (UTC)	11-11-2015 8:22
Geodetic coordinates	(49.50384 N, 5.951048 E)
Topographic elevation	310 m
Pole coordinates (x,y)	(151.418, 263.454) mas
Temperature range	(21.1÷21.8) °C
Mean barometric pressure	990.8 mbar
Vertical gravity gradient	300.9 μGal/m
He-Ne laser power	4.1 V
Accepted/total drops	338/622
Standard deviation	28.1 μGal
Combined uncertainty	4.3 μGal
Corrected mean g value	**980 949 296.2 μGal**
Expanded uncertainty (c.l. 95%)	**8.8 μGal**
Reference height	**0.487 m**
Dataset	20151302
Selected drops	100÷622
Fitting model	Linear
Measurement software	GravisoftM 2.6
Analysis libraries	ROOT v5.32.04
Analysis software	absinthDataProcess 1.2
Laser wavelength	632.9912130 nm
Clock frequency	10000000.01085 Hz
Total rise-and-fall levels	698/700
Residual s_r threshold	6 nm

Table 4: Experimental parameters and results for the site 10.

2.3.2 Site 4

For this site, the dataset taken during the day is not usable because still influenced by the movement operation from the previous site. As a matter of fact, to move from one point to the other one we need to switch off the electronics and switch on again after several minutes. The dataset 20151305 has a high number of drops and presents no strong parasitic effect. For this reason, it is used to calculate the g value in this place.

In figure 9 (right) the values of g coming from the first measurement site s10 are shown as a function of the time (i.e. the drop number). A quite stable behaviour is visible and no systematic accumulation is present. In the left panel the distribution of the values is shown together with a superimposed Gaussian fit function.

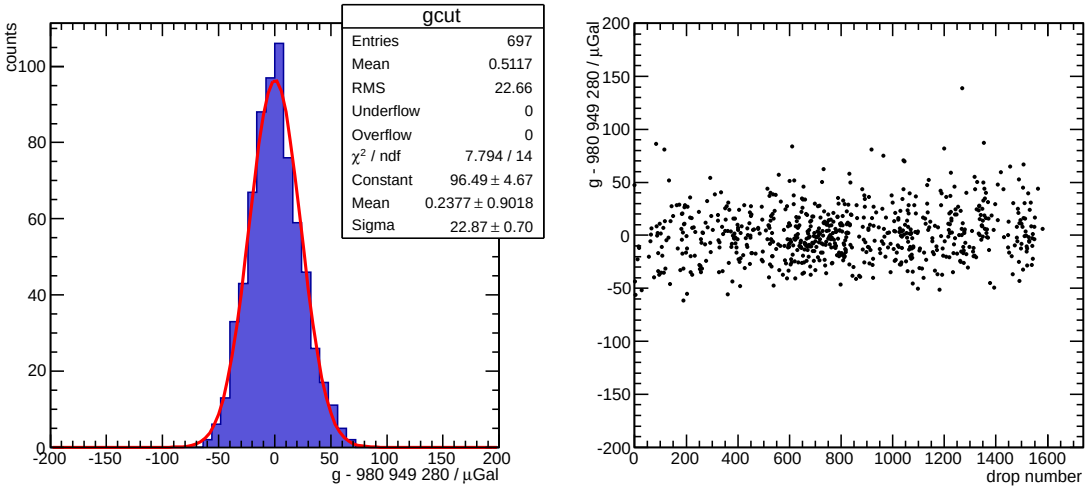

Figure 9: Experimental results for the site 4, folder 20161305. Values of g (subtracted to a nominal value for visibility) versus launch number (right). Distribution of the those values with Gaussian fit superimposed (left).

In figure 10 (left) the values of g versus the s_r of the residual distributions are shown. Because no correlation is evident, a cut on the s_r does not bias the mean value of g. In the right panel, the distribution of the s_r residuals distributions is shown. A tail for values higher than 4.2 is observable. For this reason we rejected all drops with s_r higher than 4.2 because they were not taken in the optimal instrumental and geophysical conditions. Applying such cut the distribution follows a more Gaussian behaviour.

In figure 11 the environment parameters and tide effect are shown as a function of the time. The conditions were quite stable during the whole data session.

In figure 12 it is possible to see the behaviour of four quantities used to monitor the operating of the IMGC-02 during the whole dataset a function of the drop number. The velocity is constant in time, without unexpected effects. The $h_{\mathrm{eff}}/z_{\mathrm{apex}}$ ratio is uniformly distributed around the nominal value of 1/6 used to calculate the reference height. The uncertainty due to the remaining step between rise and fall branches of the trajectory is centered at zero and is lower than ± 0.03 μGal, so as to be negligible with a respect to the final uncertainty on g. In the same way, the contribution due to terms that are proportional

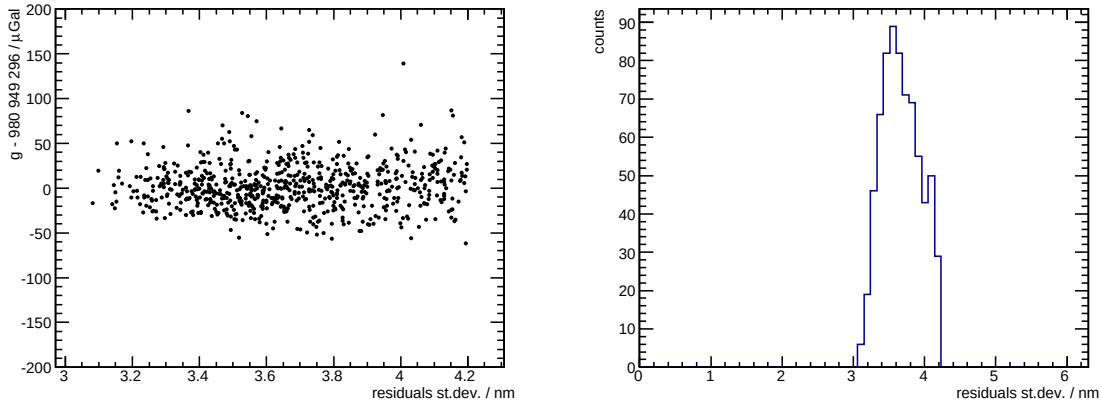

Figure 10: Experimental results for the site 4, folder 20161305. Values of g (subtracted to a nominal value for visibility) versus s_r of the residual distributions (left). Distribution of the s_r values (right).

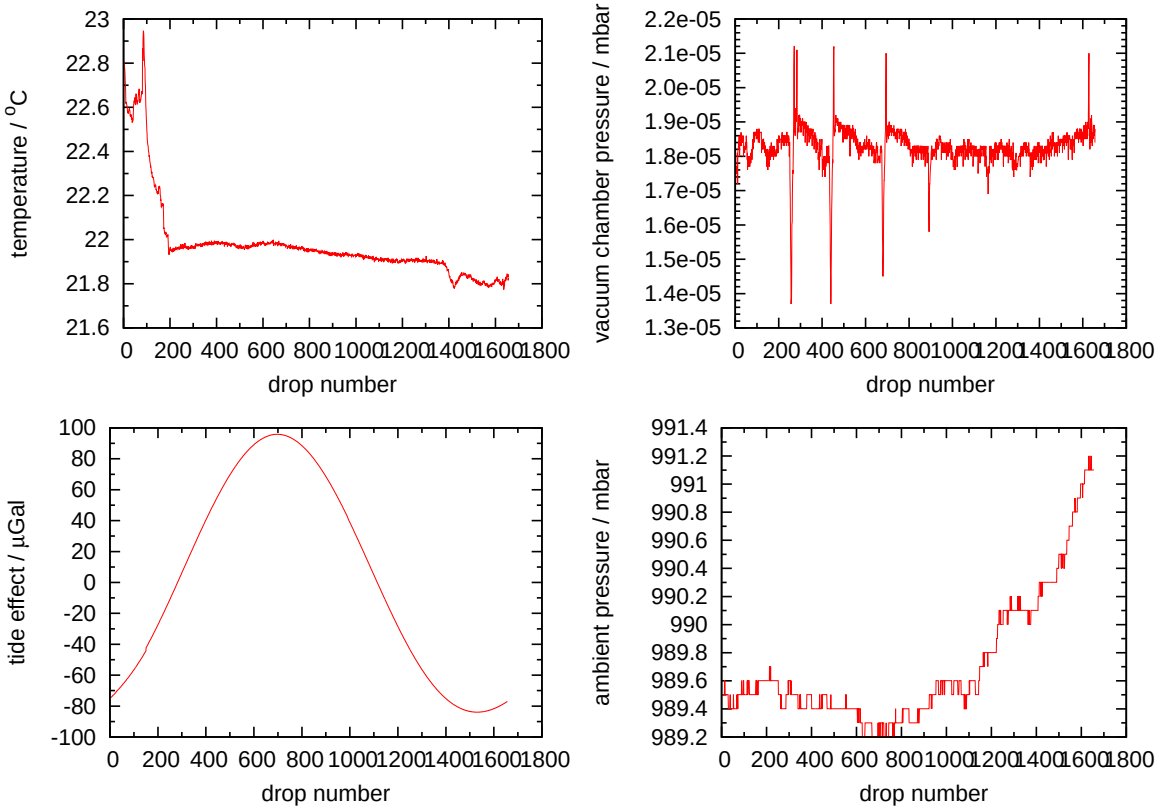

Figure 11: Experimental parameters recorded at the site 4 during the measurement session. Ambient temperature, barometric pressure and tide effect versus the drop number.

to the velocity are few order of magnitude less to the value of gravity acceleration.

As shown for the previous site, the measurement uncertainty for the site 4 is summarized in table 5. It includes the instrumental uncertainty reported in table 1.

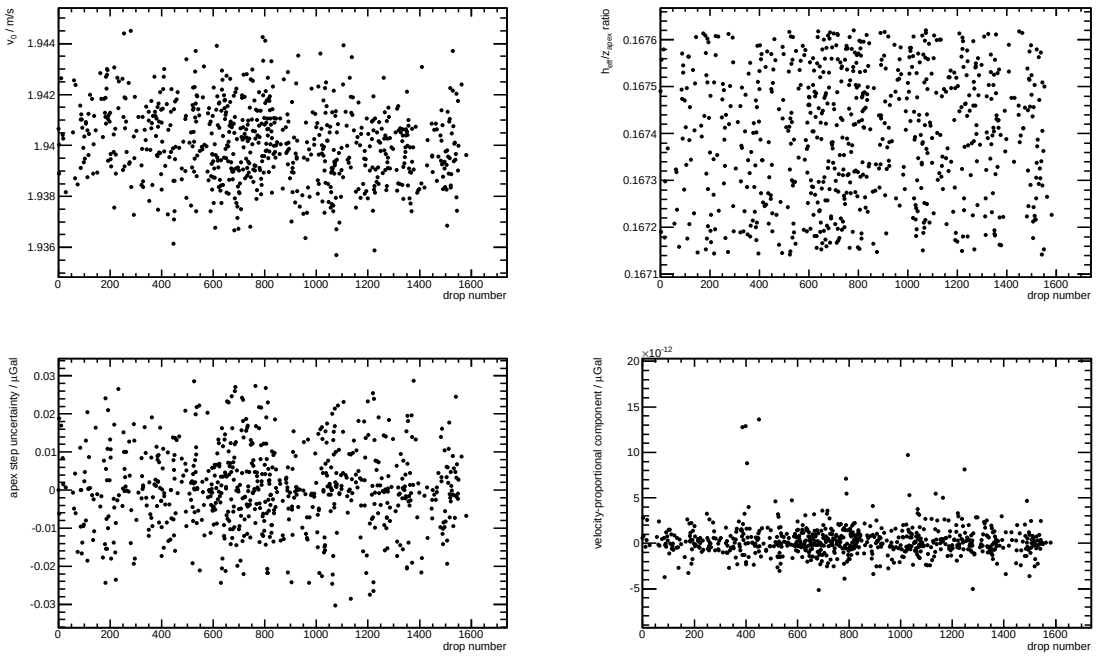

Figure 12: Measurement monitoring quantities coming from linear model algorithm for the site 4: initial velocity (up, left); ratio between the effective height and the apex vertical coordinate (up, right); uncertainty due to the remaining step between the two trajectory branches (down, left); contribution due to the component proportional to the velocity (down, right).

Measurement uncertainty for the site 4

x_i	type	corr.	a_i or s_i	$\partial y/\partial x_i$	dof	u_i / μGal
instrumental	A	0	3.7 μGal	1.0	17	3.7
Coriolis force	B - rect.	0	2.4 μGal	1.0	10	1.4
barometric pressure	B - rect.	4.3 μGal	1.0 μGal	1.0	15	0.6
tide	A	3.2 μGal	0.3 μGal	1.0	15	0.3
ocean loading	A	0	0.2 μGal	1.0	15	0.2
standard dev. mean	A	0	0.9 μGal	1.0	696	0.9
total correction		7.5 μGal				
combined uncert.						4.3 μGal
		degrees of freedom	25			
		confidence level	95%			
		coverage factor	2.1			
		expanded uncertainty	8.45 μGal			

Table 5: Final uncertainty for the absolute measurement for the site 4 in Belval. Floor recoil effect and polar motion correction (0.6 μGal) are negligible for the budget uncertainty.

In table 6 the most important results and parameters are listed for the first measurement site 4. The vertical gravity gradient calculated by the EURAMET organizers is also reported, but it was not used in the analysis of IMGC-02 data.

Summary for the site 4

Data taking start (UTC)	11-11-2015 17:15
Data taking stop (UTC)	12-11-2015 8:22
Geodetic coordinates	(49.50384 N, 5.951048 E)
Topographic elevation	310 m
Pole coordinates (x,y)	(151.418, 263.454) mas
Temperature range	(21.1÷21.8) °C
Mean barometric pressure	990.8 mbar
Vertical gravity gradient	301.7 μGal/m
He-Ne laser power	4.1 V
Accepted/total drops	697/1655
Standard deviation	22.6 μGal
Combined uncertainty	4.1 μGal
Corrected mean g value	**980 949 280.4 μGal**
Expanded uncertainty (c.l. 95%)	**8.45 μGal**
Reference height	**0.488 m**
Dataset	20151305
Selected drops	0÷1600
Fitting model	Linear
Measurement software	GravisoftM 2.6
Analysis libraries	ROOT v5.32.04
Analysis software	absinthDataProcess 1.2
Laser wavelength	632.9912130 nm
Clock frequency	10000000.01085 Hz
Total rise-and-fall levels	698/700
Residual s_r threshold	4.2 nm

Table 6: Experimental parameters and results for the site 4.

2.3.3 Site 7

The first two datasets taken in this site, 20151306 and 20151307, are influenced by some tests we made during the day in order to improve the stability of the measurements and to check for possible parasitic effects. The dataset 20151308 presents no problem in term of stability and performance, so it was used to compute the value of local acceleration g.

In figure 13 (right) the values of g coming from the first measurement site s10 are shown as a function of the time (i.e. the drop number). A quite stable behaviour is visible and no systematic accumulation is present. In the left panel the distribution of the values is shown together with a superimposed Gaussian fit function.

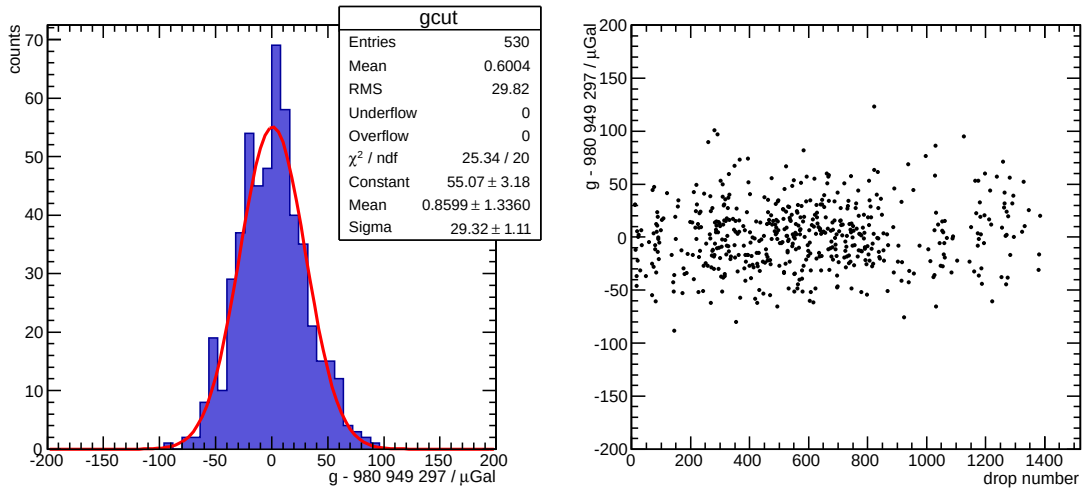

Figure 13: Experimental results for the site 7, folder 20161308. Values of g (subtracted to a nominal value for visibility) versus launch number (right). Distribution of the those values with Gaussian fit superimposed (left).

In figure 14 (left) the values of g versus the s_r of the residual distributions are shown. Because no correlation is evident, a cut on the s_r does not bias the mean value of g. In the right panel, the distribution of the s_r residuals distributions is shown. A tail for values higher than 4.6 is observable. For this reason we rejected all drops with s_r higher than 4.6 because they were not taken in the optimal instrumental and geophysical conditions. Applying such cut the distribution follows a more Gaussian behaviour.

In figure 15 it is possible to see the behaviour of four quantities used to monitor the operating of the IMGC-02 during the whole dataset a function of the drop number. The velocity is constant in time, without unexpected effects. The $h_{\text{eff}}/z_{\text{apex}}$ ratio is uniformly distributed around the nominal value of 1/6 used to calculate the reference height. The uncertainty due to the remaining step between rise and fall branches of the trajectory is centered at zero and is lower than ± 0.03 μGal, so as to be negligible with a respect to the final uncertainty on g. In the same way, the contribution due to terms that are proportional to the velocity are few order of magnitude less to the value of gravity acceleration.

In figure 16 the environment parameters and the tide effect are shown as a function of the time. The conditions were quite stable during the whole data session.

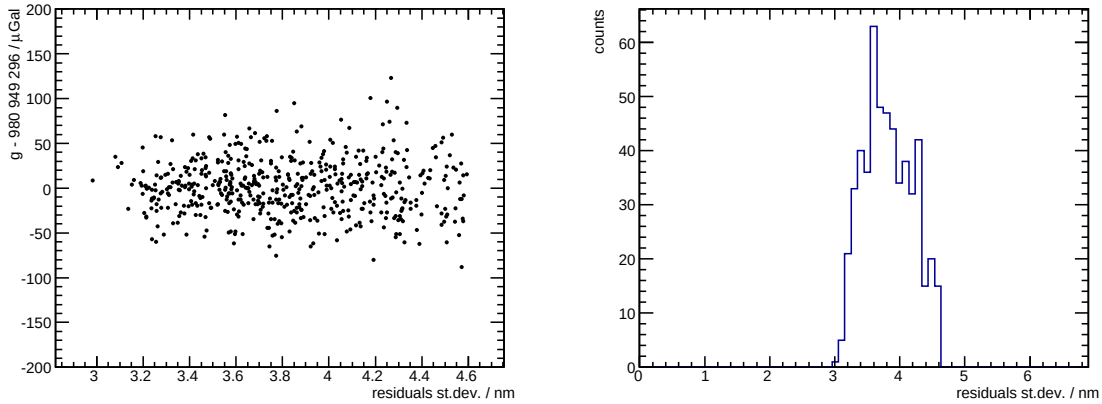

Figure 14: Experimental results for the site 10, folder 20161302. Values of g (subtracted to a nominal value for visibility) versus s_r of the residual distributions (left). Distribution of the s_r values (right).

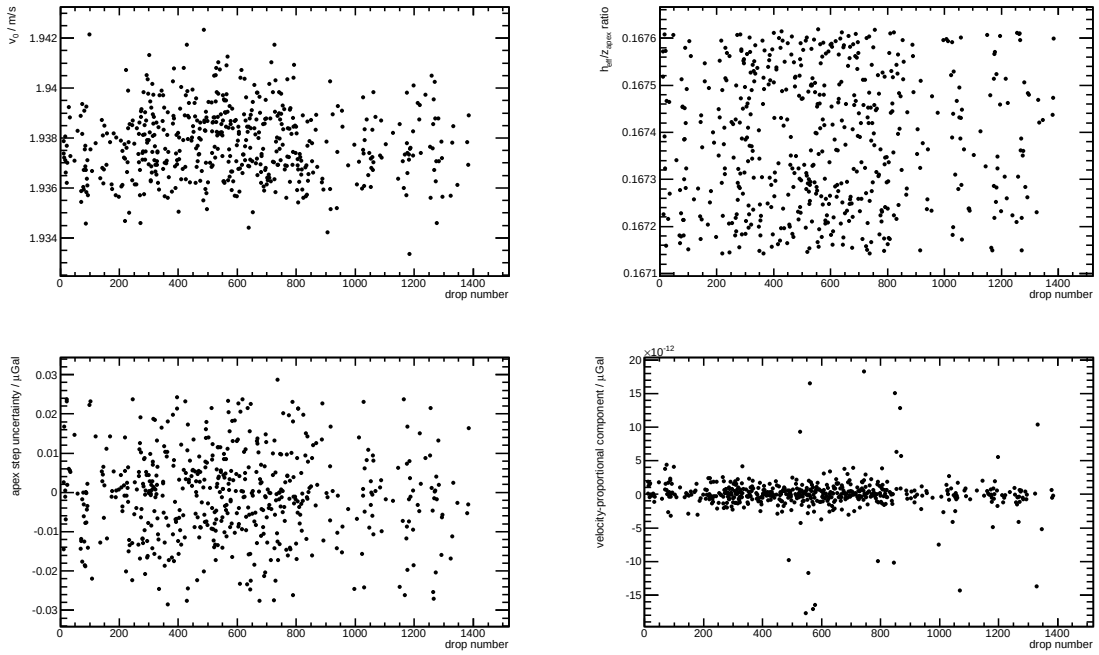

Figure 15: Measurement monitoring quantities coming from linear model algorithm for the site 4: initial velocity (up, left); ratio between the effective height and the apex vertical coordinate (up, right); uncertainty due to the remaining step between the two trajectory branches (down, left); contribution due to the component proportional to the velocity (down, right).

The measurement uncertainty for the site 4 is summarized in table 7. It includes the instrumental uncertainty reported in table 1.

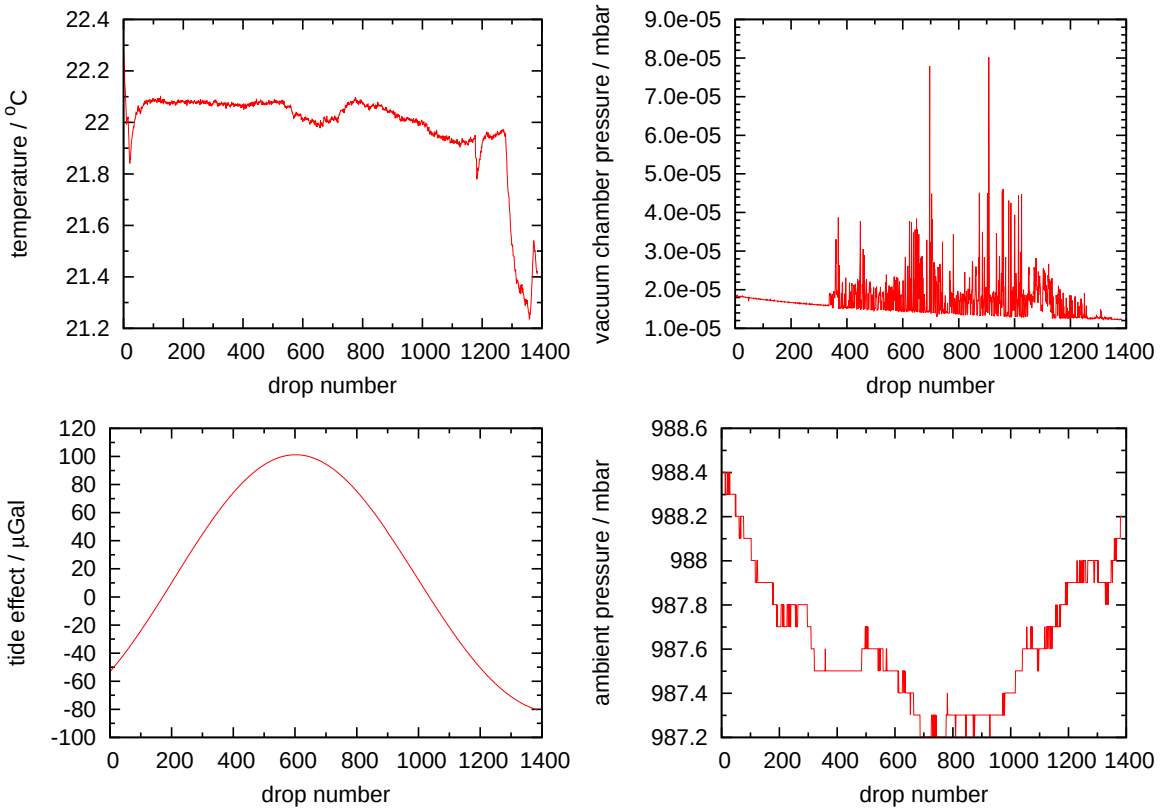

Figure 16: Experimental parameters recorded at the site 7 during the measurement session. Ambient temperature, barometric pressure and tide effect versus the drop number.

Measurement uncertainty for the site 7

x_i	type	corr.	a_i or s_i	$\partial y/\partial x_i$	dof	u_i / μGal
instrumental	A	0	3.7 μGal	1.0	17	3.7
Coriolis force	B - rect.	0	2.4 μGal	1.0	10	1.4
barometric pressure	B - rect.	3.7 μGal	1.0 μGal	1.0	15	0.58
tide	A	24.0 μGal	0.3 μGal	1.0	15	0.3
ocean loading	A	0	0.2 μGal	1.0	15	0.2
standard dev. mean	A	0	1.3 μGal	1.0	529	1.3
total correction		27.7 μGal				
combined uncert.						4.2 μGal
		degrees of freedom	27			
		confidence level	95%			
		coverage factor	2.1			
		expanded uncertainty	8.6 μGal			

Table 7: Final uncertainty for the absolute measurement for the site 7 in Belval. Floor recoil effect and polar motion correction (0.6 μGal) are negligible for the budget uncertainty.

In table 8 the most important results and parameters are listed for the first measurement site 7. The vertical gravity gradient calculated by the EURAMET organizers is also reported, but it was not used in the analysis of IMGC-02 data.

Summary for the site 7

Data taking start (UTC)	12-11-2015 17:36
Data taking stop (UTC)	13-11-2015 6:56
Geodetic coordinates	(49.50384 N, 5.951048 E)
Topographic elevation	310 m
Pole coordinates (x,y)	(151.418, 263.454) mas
Temperature range	(21.1÷21.8) °C
Mean barometric pressure	990.8 mbar
Vertical gravity gradient	295.8 μGal/m
He-Ne laser power	4.1 V
Accepted/total drops	530/1385
Standard deviation	29.8 μGal
Combined uncertainty	4.2 μGal
Corrected mean g value	**980 949 297.3 μGal**
Expanded uncertainty (c.l. 95%)	**8.6 μGal**
Reference height	**0.489 m**
Dataset	20151308
Selected drops	0÷1400
Fitting model	Linear
Measurement software	GravisoftM 2.6
Analysis libraries	ROOT v5.32.04
Analysis software	absinthDataProcess 1.2
Laser wavelength	632.9912130 nm
Clock frequency	10000000.01085 Hz
Total rise-and-fall levels	698/700
Residual s_r threshold	4.6 nm

Table 8: Experimental parameters and results for the site 7.

2.4 Cross-check measurements at INRiM

In order to check for the good performance of the absolute gravimeters, we usually perform several measurement sessions at the gravity laboratory of INRiM in the weeks before and after the one dedicated to the comparison.

We do not report here the result of those measurements because they are out of the aim of such technical report. However, several problems were found. The standard deviation of the values was larger than the expected one and the final value of g differs from the nominal one measured at the same laboratory.

After a dedicated investigation, we suppose that the source of the problem is referred to a not optimal centering of the test object [3]. We estimated an additional uncertainty contribution of 7 μGal to take into account for this aspect. The combined standard uncertainty must then enlarged from about 4.3, 4.1 and 4.2 to 8.2, 8.1 and 8.2 μGal.

3 Conclusion

The IMGC-02 participated to the EURAMET.M.G-K2 regional comparison of absolute gravimeters. Using three days of data measurements, is was possible to compute a value of the absolute local acceleration of gravity in all the tree sites dedicated by the organizers to the IMGC-02.

The instrument worked well in all the sites, even if the floor and building conditions are not optimized for high-precision gravity measurements.

Data were processed and corrected at INRiM together with the evaluation of the uncertainty budget. The values were then communicated to the comparison organizers to be used for the determination of the Key Value and for the Pilot Study.

The final values are referable to an effective height of about 0.488 m. They are the following ones:

- for site 10: $g =$ (980 949 296.2 $\pm$ 16.4) μGal
- for site 4: $g =$ (980 949 280.4 $\pm$ 16.2) μGal
- for site 7: $g =$ (980 949 297.3 $\pm$ 16.4) μGal

where the expanded uncertainty is calculated using the coverage factor for a confidence level of 95% .

References

[1] D'Agostino G, Desogus S, Germak A, Origlia C, Quagliotti D, Berrino G, Corrado G, d'Errico V and Ricciardi G, *The new IMGC-02 transportable absolute gravimeter: measurement apparatus and applications in geophysics and volcanology*, Ann. Geophys. **51** (2008) 3949

[2] Biolcati E, Desogus S, Mazzoleni F, Origlia C, Vitiello F, *Modifiche apportate al gravimetro assoluto IMGC-02*, INRiM - RT 37/2012

[3] Germak A, Desogus S, Origlia C, *Interferometer for the IMGC rise-and-fall absolute gravimeter*, Metrologia, Special issue on gravimetry, Bureau Int Poids Mesures, BIPM, Pavillon De Breteuil, F-92312, Svres Cedex, France, 2002, Vol. 39, Nr. 5, pp. 471-475

[4] D'Agostino G, Germak A, Desogus S, Barbato G, *A Method to Estimate the Time-Position Coordinates of a Free-Falling Test-Mass in Absolute Grvimetry*, Metrologia Vol. 42, No. 4, pp. 233-238, August 2005.

[5] Nagorny V, Biolcati E, Svitlov S., *Enabling a linear model for the IMGC-02 absolute gravimeter*, Metrologia, 51, 3

[6] Brun R. Rademakers F., *ROOT - An Object Oriented Data Analysis Framework*, Proceedings AIHENP'96 Workshop, Lausanne, Sep. 1996, Nucl. Inst. & Meth. in Phys. Res. A 389 (1997) 81-86. `root.cern.ch`

[7] International Earth Rotation and Reference System Service (IERS), *Bulletin B 335 1 January 2016*, `ftp://hpiers.obspm.fr/iers/bul/bulb_new/bulletinb.335`

[8] *Evaluation of measurement data Guide to the expression of uncertainty in measurement*, JCGM 100:2008 (GUM 1995 with minor corrections)

[9] Biolcati E, Svitlov S, Germak A, *Self-attraction effect and correction on three absolute gravimeters*, Metrologia **49** (2012) 560566

[10] Z Jiang *et al.*, *Final report on the Seventh International Comparison of Absolute Gravimeters (ICAG 2005)*, Metrologia **48** (2011) 246

[11] Francis O *et al*, *CCM.G-K2 key comparison*, Metrologia 52 (2015) 07099